Journal of Microscopy, Vol. 210, Pt 1 April 2003, pp. 74–79
Received 5 May 2002; accepted 10 January 2003

Electron energy-loss spectroscopy study of thin film hafnium aluminates for novel gate dielectrics

S. STEMMER, Z. Q. CHEN, W. J. ZHU* & T. P. MA*
Materials Department, University of California, Santa Barbara, CA 93106–5050, U.S.A.
**Department of Electrical Engineering, Yale University, New Haven, CT 06520, U.S.A.*

Key words. Gate dielectrics, electron energy-loss spectroscopy, HfO_2, transition metal oxides.

Summary

We have used conventional high-resolution transmission electron microscopy and electron energy-loss spectroscopy (EELS) in scanning transmission electron microscopy to investigate the microstructure and electronic structure of hafnia-based thin films doped with small amounts (6.8 at.%) of Al grown on (001) Si. The as-deposited film is amorphous with a very thin (~0.5 nm) interfacial SiO_x layer. The film partially crystallizes after annealing at 700 °C and the interfacial SiO_2-like layer increases in thickness by oxygen diffusion through the Hf-aluminate layer and oxidation of the silicon substrate. Oxygen K-edge EELS fine-structures are analysed for both films and interpreted in the context of the films' microstructure. We also discuss valence electron energy-loss spectra of these ultrathin films.

Introduction

Thin films of transition metal oxides with dielectric constants (k) greater than that of SiO_2 ($k = 3.9$) are currently investigated as novel gate dielectric materials in complementary metal-oxide–semiconductor (CMOS) devices (Kingon *et al.*, 2000; Wilk *et al.*, 2001). High-k metal oxides that are potentially stable in contact with silicon include HfO_2 and ZrO_2, and their alloys with SiO_2 (silicates) and Al_2O_3 (aluminates), respectively (Hubbard & Schlom, 1996). High-k films are typically amorphous in their as-deposited state but crystallize during high-temperature anneals that are required for device processing. Crystallization is believed to be correlated with an undesired increase in leakage currents (Kwo *et al.*, 2001; Zhu *et al.*, 2001). Alloying the binary oxides with SiO_2 or Al_2O_3 is used to increase the crystallization temperatures (Neumayer & Cartier, 2001; van Dover *et al.*, 2001; Zhu *et al.*, 2001). While the electronic structure of bulk, crystalline ZrO_2 and HfO_2 has been investigated experimentally (McComb *et al.*, 1992; French *et al.*, 1994; McComb, 1996; Lim *et al.*, 2002), less is known about that of silicates and aluminates, and those of amorphous thin-film dielectrics. For example, single-phase Zr- or Hf-aluminates that are of interest for gate dielectrics are typically metastable and cannot be synthesized using traditional ceramic sintering processes that involve high processing temperatures. Thin films might have electronic structures different from their bulk counterparts because they can accommodate significant amounts of non-stoichiometry and structural disorder.

Electron energy-loss spectroscopy (EELS) is a powerful technique to analyse the unoccupied states above the Fermi level with subnanometre spatial resolution. The energy-loss near-edge fine structure (ELNES) results when the incoming electron excites a core level electron into an unoccupied state above the Fermi level (Egerton, 1996) and thus probes the site and symmetry projected density of states. The low-loss ('valence loss') region of the EELS spectrum (0–100 eV) reflects collective valence electron excitations (plasmons) and single valence electron excitations into unoccupied states in the conduction band (Egerton, 1996) and can thus be compared with vacuum ultraviolet (VUV) reflectance spectroscopies.

The crystal and electronic structure and the physical properties of HfO_2 are similar to those of ZrO_2. Both oxides show phase transformations from monoclinic to tetragonal to cubic as the temperature increases. Doping with trivalent ions stabilizes the higher symmetry phases at low temperatures. In the purely ionic model, the Zr 4d bands and Hf 5d bands, respectively, are empty, and the O 2p bands are fully occupied, due to the $4d^0$ and $5d^0$ electronic configurations, respectively. Electronic structure calculations of partial densities of states also show that the upper valence band is formed by the O 2p states and the lowest conduction band is formed mainly by the cation d-states (Medvedeva *et al.*, 1990; Soriano *et al.*, 1995; de Boer & de Groot, 1998; Kralik *et al.*, 1998; Jomard *et al.*, 1999). At higher energies, bands are formed from O 2p mixed with metal $(n + 1)sp$ states ($n = 4$ for ZrO_2 and $n = 5$ for HfO_2).

Correspondence: Dr S. Stemmer. E-mail: stemmer@mrl.ucsb.edu

X-ray absorption (XAS) and EELS studies of oxygen K-edges of crystalline HfO_2 and ZrO_2, corresponding to transitions from the 1*s* oxygen core states to the lowest conduction bands, show two characteristic sharp features near the absorption edge (Rowley & Graham, 1993; Soriano *et al.*, 1993; McComb, 1996; Chen, 1997). In the absence of any *p*–*d* hybridization, there should be no intensity in peaks in the energy-loss spectrum that are due to transitions into *d*-bands, because the $s \rightarrow d$ transition is forbidden by the dipole selection rule (Egerton, 1996). The intensity at the oxygen K-edge onset is therefore explained with a hybridization of metal *n*d and oxygen 2*p* states (Rowley & Graham, 1993; Soriano *et al.*, 1993; Chen, 1997).

In Al_2O_3, the upper valence band is derived from O 2*p* states and the conduction band is derived from Al 3*s* and 3*p* states. The lowest unoccupied bands of alloys of the binary transition metal oxides with Al_2O_3 or SiO_2 are expected to be formed by the transition metal *d*-states, which lie lower in energy than the unoccupied states of Si and Al. For example, XAS and ELNES studies of the oxygen K-edges of zircon ($ZrSiO_4$) show that the edge onset is associated with transitions to zirconium 4*d* empty states hybridized with oxygen 2*p* orbitals (McComb *et al.*, 1992; Wu & Seifert, 1996). Transitions at higher energy losses are associated with transitions into silicon 3*s*/3*p* orbitals hybridized with O 2*p* orbitals and zirconium 5*s* and 5*p* orbitals (McComb *et al.*, 1992). Therefore, the band offsets with Si, which determine the device performance, are determined by the energy levels of the transition metal *d*-states and the oxygen 2*p* band, respectively (Lucovsky, 2002). Investigation of the unoccupied *d*-bands in high-*k* oxides and their alloys is therefore of great practical importance (Lim *et al.*, 2002; Lucovsky, 2002).

In this paper, we use EELS to investigate the electronic structure of as-deposited and annealed jet vapour-deposited Hf-aluminate gate dielectric films using ELNES of oxygen K-edges and valence loss EELS (VEELS) spectra. We also report microstructure changes associated with annealing.

Experimental

$Hf_{1-x}Al_xO_{2-x/2}$ films with $x = 0.068$ were deposited by jet vapour deposition (JVD) at room temperature on HF-last Si substrates. Hf and Al vapour were generated by dc sputtering in separate nozzles and were brought into the deposition chamber by a supersonic Ar jet. A supersonic jet of O_2 was also brought into the deposition chamber from a separate nozzle. Details of the deposition process are described elsewhere (Ma, 1998). X-ray photoelectron spectroscopy was used to confirm the composition of the films. The electrical and structural properties of as-deposited and annealed samples, respectively, were investigated. Post-deposition annealing was performed for 2 min in N_2 at 700 °C. Note that the nitrogen gas annealing atmosphere contains sufficient oxygen (> 1 p.p.m., corresponding to an oxygen partial pressure of $> 10^{-4}$ torr) to cause interfacial SiO_2 formation by oxidation of the silicon substrate if oxygen diffuses through the high-*k* film (Stemmer *et al.*, 2002). Al was used as a back electrode and Pt was e-beam evaporated as top electrode for electrical measurements. After electrode deposition, the samples were annealed at 150 °C (as-deposited) and 300 °C (annealed), respectively, in N_2 to improve Pt adhesion. Details of the electrical measurements will be reported elsewhere. The equivalent oxide thickness (EOT), defined as the thickness of the high-*k* dielectric scaled by the ratio of its dielectric constant to that of silicon dioxide, was less than 1.1 nm after deposition and increased to ~1.6 nm after annealing at 700 °C.

Transmission electron microscopy (TEM) samples were prepared by standard cross-section preparation techniques, with Ar ion-milling as a final step. The film microstructure and chemistry were investigated using a 200-kV transmission electron microscope (JEOL JEM 2010F) equipped with a field-emission gun, an annular dark-field detector and a post-column imaging filter (Gatan GIF200). This microscope is capable of achieving sub 0.2-nm probe sizes in scanning transmission electron microscopy (STEM) for microanalysis and incoherent Z-contrast (or high-angle annular dark-field, ADF) lattice imaging (James *et al.*, 1998). EELS analysis across the gate stack was performed in STEM mode by positioning a 0.2-nm probe at different locations in the ADF image of the stack and subsequently recording a spectrum. The energy resolution (full width at half maximum) measured at the zero-loss peak was about 1 eV. Details of the acquisition parameters are given in the figure captions. No deconvolution of the spectra was performed. All spectra were dark current and gain corrected.

Results and discussion

Microstructure

Figure 1(a) shows a conventional high-resolution TEM (HRTEM) micrograph of the as-deposited $Hf_{0.932}Al_{0.068}O_{1.966}$ film. An interfacial SiO_x layer, brighter in contrast and about 0.5 nm thick, can also be observed. This interfacial layer appears dark in the ADF image (inset in Fig. 1a), due to the lower atomic number of Si compared to Hf. The SiO_2-like nature of the interfacial layer, as opposed to a silicate, can be verified using the ELNES of the oxygen K-edge (see section below). The film appeared amorphous across the entire TEM sample. In contrast, the film annealed at 700 °C showed crystallization in some regions of the film and amorphous structure in others. Figure 1(b) shows an HRTEM micrograph of an area where lattice fringes are visible in the film. Fast Fourier transforms (FFTs) showed that the lattice plane spacing in the film was different from that of the Pt electrode, and thus ensured that lattice fringes in the film are not an artefact due to delocalization of Pt lattice fringes in the image due to the coherent nature of the field-emission source (Otten & Coene, 1993). Figure 1(b) also shows that the interfacial SiO_2 layer

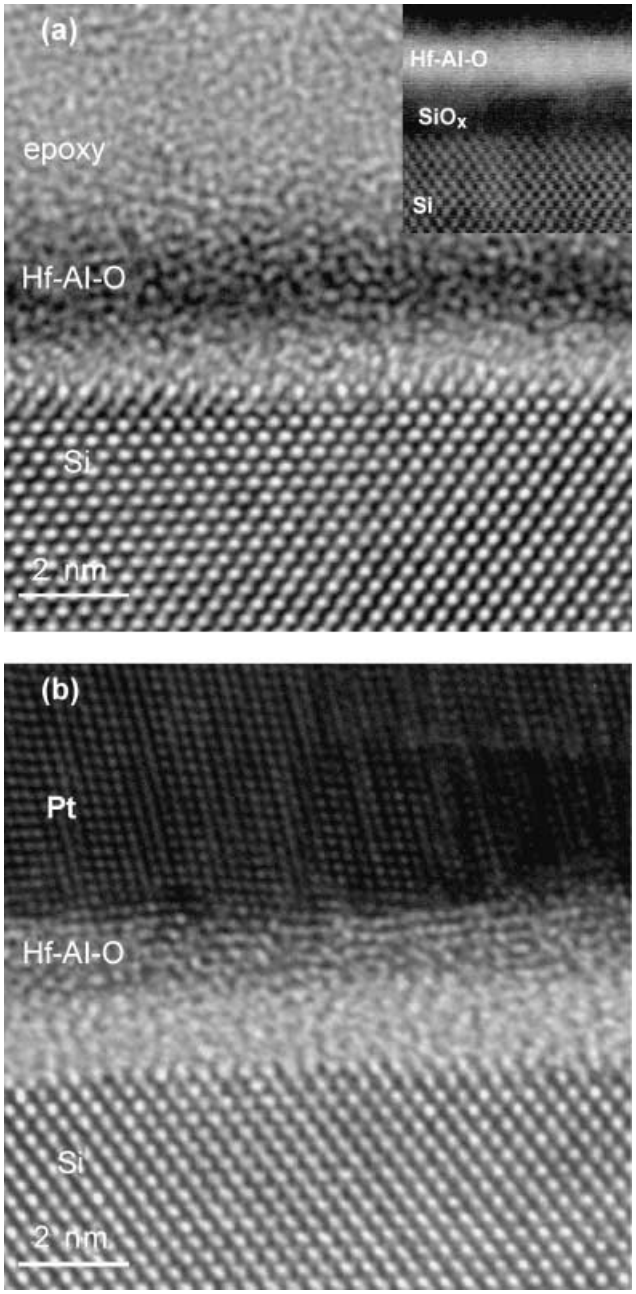

Fig. 1. (a) Cross-section HRTEM micrograph of the as-deposited $Hf_{0.932}Al_{0.068}O_{1.966}$ film. The inset shows an ADF image. (b) Cross-section HRTEM micrograph of the sample after annealing at 700 °C, recorded from a region underneath the patterned Pt electrode.

has grown in thickness to ~1.6 nm during annealing, most likely by oxygen diffusion through the Hf-aluminate film. Growth of a low-permittivity, interfacial SiO_2 connected in series with the high-*k* film is the likely origin for the increase in the EOT measured after annealing.

With respect to the crystallizing phase, the Hf-aluminates are expected to behave similar to Zr-aluminates. For the latter system, equilibrium and metastable phase diagrams have

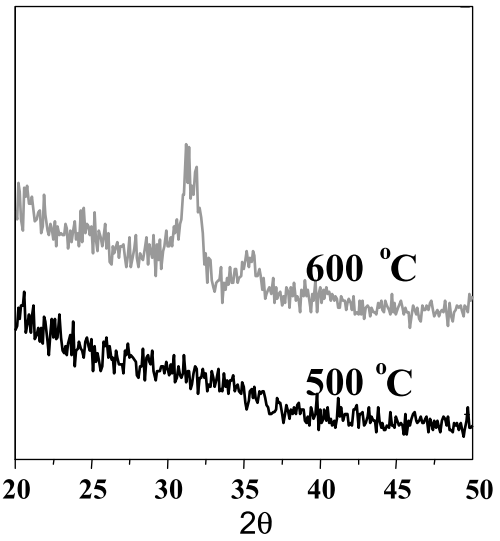

Fig. 2. Grazing incidence X-ray diffraction scan using Cu Kα radiation of 100-nm-thick $Hf_{0.932}Al_{0.068}O_{1.966}$ annealed for 2 min in nitrogen at 500 and 600 °C, respectively, showing onset of crystallization at temperatures above 600 °C. The reflections can be assigned to monoclinic hafnia.

been reported in the literature. The equilibrium solubility of Al_2O_3 in ZrO_2 is limited due to the small size of Al^{3+} compared to Zr^{4+}, and is negligible at temperatures below 900 °C. At room temperature, a two-phase microstructure, consisting of monoclinic ZrO_2 and α-Al_2O_3, is predicted from the equilibrium phase diagram (Lakiza & Lopato, 1997). However, investigators have reported the crystallization of metastable phases with extended solid solubilities from amorphous precursors in several oxide systems, including ZrO_2–Al_2O_3 (Levi, 1998). Crystallization to a single phase of tetragonal $(Zr,Al)O_2$ was observed for compositions with up to 40 mol% Al_2O_3 ($x = 0.57$ in the notation used above) and temperatures up to 900 °C (Balmer *et al.*, 1994). Given the relatively low annealing temperatures and the small concentration of Al in this study, we therefore expect crystallization to a single, metastable crystalline HfO_2 phase with Al in solid solution. Grazing incidence X-ray diffraction scans of thicker films (~100 nm) showed onset of crystallization with peaks appearing at $2\theta \approx 31.5°$ and 35° for samples annealed at 600 °C and above, corresponding to the 111 and 200 reflections, respectively, of tetragonal or monoclinic hafnia and no peaks that could be assigned to alumina (Fig. 2). EELS investigations, described below, further confirmed that both as-deposited and annealed films are compositionally homogenous, and partially crystallized in the annealed film.

Electronic structure

Figure 3 shows EELS oxygen K-edges recorded from the as-deposited film (Fig. 3a), the annealed film (Fig. 3b) and the interfacial SiO_x-like layer (Fig. 3c), respectively. Edges from

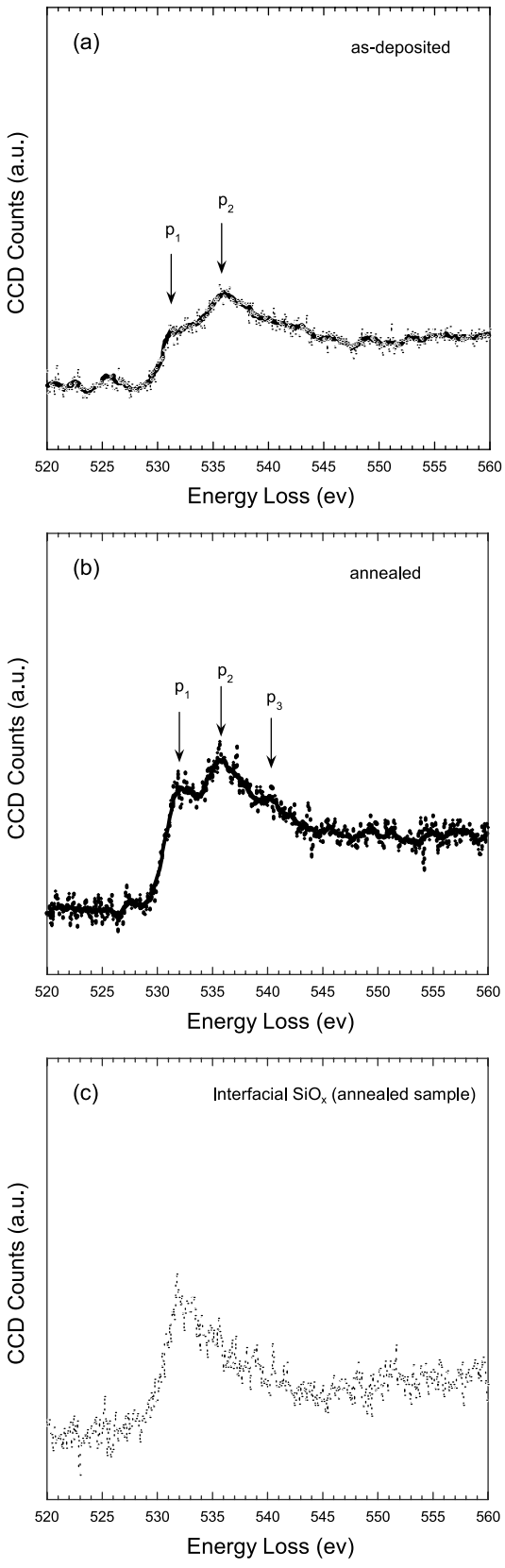

both films show characteristic double peaks (p_1 and p_2) at the edge onset, similar to bulk, crystalline HfO_2. The peaks are wider in the as-deposited film and thus appear less well resolved. The splitting between the two peaks is about 4.2 (as-deposited) and 3.8 eV (annealed sample), respectively. Given our energy resolution the splitting is in the same range as the one measured by other authors for pure HfO_2 (Soriano *et al.*, 1993; Chen, 1997). Other authors have shown that in transition metal oxide films with oxygen deficiency or excess oxygen, the p_1–p_2 peak splitting would be absent (Ramanathan *et al.*, 2001; Busch *et al.*, 2002). In contrast, the oxygen K-edge ELNES of the interfacial layers (dark layers in ADF) show no peak splitting and a fine-structure typical for SiO_2 (Wallis *et al.*, 1995).

It is interesting to note that the as-deposited film shows two peaks at the edge onset despite its amorphous nature. Thus p_1 and p_2 must reflect the nearest neighbour co-ordination and are little affected by the absence of long-range order. For cubic hafnia (and zirconia), the p_1 and p_2 peaks are interpreted to reflect the splitting of the *d*-bands by the crystal field due to an eight-fold co-ordination of the cations to form e_g and t_{2g} subbands via the *p*–*d* hybridization. Electronic structure calculations of cubic and tetragonal zirconia and hafnia show two *d*-subbands (Kralik *et al.*, 1998; Ostanin *et al.*, 2000; Peacock & Robertson, 2002). It is therefore tempting to interpret the presence of the double peaks in the amorphous film as short-range order in which Hf is in nearly symmetrical eight-fold co-ordination with oxygen. However, the *d*-band in monoclinic zirconia (and likely hafnia) where the metal has seven-fold coordination is degenerated (French *et al.*, 1994), but experimental and calculated EELS and XAS spectra of the monoclinic polymorph still show the characteristic double-peaks (Ostanin *et al.*, 2000).

With respect to the differences in the oxygen K-edge fine-structures between the as-deposited and annealed film, either structural rearrangements or changes in the point defect chemistry can be responsible. McComb *et al.* have shown that in crystalline ZrO_2 the separation as well as the depth of the minimum between the first two peaks reflects the specific polymorph (cubic, tetragonal or monoclinic) and the doping concentration (McComb, 1996; Vlachos *et al.*, 2001). Similar trends are likely for HfO_2 polymorphs. Although no experimental data are yet available to support this, calculated band structures of cubic ZrO_2 and HfO_2 are similar, except for a greater splitting of the Hf 5*d* conduction band states (Demkov, 2001; Peacock & Robertson, 2002). Theoretical calculations

Fig. 3. EELS oxygen K-edges of (a) the as-deposited film, (b) the film after annealing at 700 °C, and (c) the interfacial SiO_2 in the annealed sample. EELS spectra were acquired in STEM mode with an exposure time of 8 s, and an energy dispersion of 0.1 eV per channel. The oxygen K-edges shown here are a sum of three (a), five (b) and two (c) spectra, respectively. Solid dots represent the raw experimental data after background subtraction and summation. The solid lines are the same spectra after smoothing using a 1-eV filter in the Gatan software.

of oxygen K-edges of undoped ZrO_2 polymorphs show that an increase in symmetry is associated with a greater peak splitting and narrower peaks (Ostanin *et al.*, 2000). A greater symmetry of the Hf-O polyhedra in the annealed film, for example due to crystallization and more equal bond lengths, would cause p_1 and p_2 to become more narrow with a more pronounced gap between the peaks, as is observed. The annealing temperature was sufficient to allow for structural rearrangements, because the annealed film is partially crystallized. Similar changes in the ELNES should also take place with a reduction in the point defect concentration. Doping of zirconia with trivalent yttrium, which introduces oxygen vacancies for charge neutrality reasons, causes the gap between p_1 and p_2 to fill and also a shift of p_2 to higher energies (Ostanin *et al.*, 2000, 2002). Here, the Al dopant concentration is expected to be the same for both films. Al substitution on Hf sites should introduce oxygen vacancies into the lattice, similar to Y doping, for charge compensation. Defect reactions that might potentially take place during annealing can be very complex. They include filling of oxygen vacancies by oxygen present in the annealing atmosphere, segregation of Al to grain boundaries, and formation of complex defect associates (Guo, 2001). In particular, filling of oxygen vacancies could have taken place during annealing, as enough oxygen was present in the annealing atmosphere to form additional SiO_2 at the interface. Further investigations, including modelling of the EELS spectra, are necessary to investigate the influence of such complex changes in the point defect chemistry on the oxygen K-edges ELNES.

Figure 4 shows VEELS spectra of the annealed film and the interfacial SiO_2. The energy of the intensity threshold in the Hf-aluminate film, which is a measure of the band gap, is around 5 eV. The film shows two peaks at ~16 eV (peak A) and 24–25 eV (peak B). The peaks between 31 and 38 eV are the Hf $O_{2,3}$ edge. In contrast to ZrO_2, no quantitative assignments of peaks in the low-loss region of bulk hafnia exist in the iterature, although low-loss spectra of the two materials are very similar (Ahn & Krivanek, 1983). Following the assignments made for ZrO_2, peak A corresponds to a bulk plasmon of HfO_2. Some controversy exists regarding the interpretation of peak B for ZrO_2 (Camagni *et al.*, 1994). In the Hf-aluminate films, the position of this peak varied between 23 and 26 eV. Different degrees of overlap with the plasmon signal of the interfacial SiO_2 (~22 eV) or the Pt electrodes (~23 eV) are a possible explanation. Other authors have observed a delocalization of the low-loss EELS signal of up to 4 nm in ZrO_2 (Suenaga *et al.*, 1998), which is greater than the Hf-aluminate film thickness. Other explanations include variations in the composition of the film. Furthermore, the height of peak B is greater than that of peak A, contrary to what is observed in bulk HfO_2 and ZrO_2. This might be due to overlap with the plasmon signal from the adjacent layers, or due to the influence of the Al dopant. Qualitatively, the low-loss spectra obtained here look similar to those of an alumina/zirconia interface (Suenaga *et al.*, 1998), which supports this interpretation.

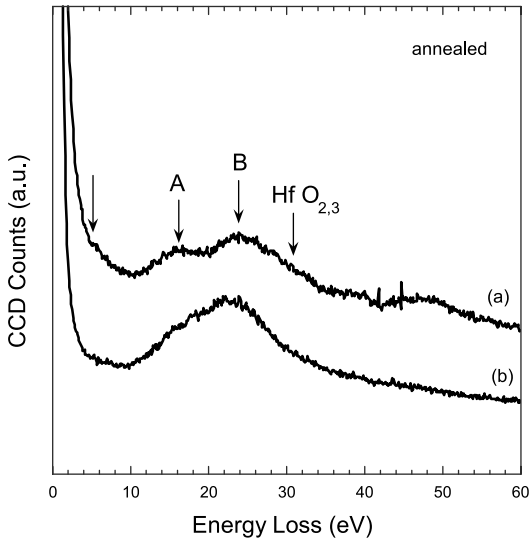

Fig. 4. Low-loss EELS spectra of (a) the annealed Hf-aluminate film and (b) the interfacial SiO_2 in the annealed sample. The zero-loss peak is to the left. Spectra were acquired with an exposure time of 0.02 s and an energy dispersion of 0.1 eV per channel. The spectrum in (a) is the sum of four spectra, the spectrum (b) is the sum of two spectra. Besides summation of individual spectra, no other data processing was performed. The arrow on the left indicates the onset of intensity in the Hf-aluminate film.

Conclusions

In summary, we have shown that the oxygen K-edge ELNES of amorphous Hf-aluminate films grown by JVD show features at the edge onset that represent the unoccupied metal *d*-states. The as-deposited and an annealed film exhibited characteristic double peaks at the edge onsets. The presence of these peaks in an amorphous film also showed that they represent the nearest neighbour Hf-O bonds. We showed that the oxygen K-edge ELNES is sensitive to processing of the high-*k* films. Annealing at 700 °C causes the films partially to crystallize and the *d*-state features of the oxygen K-edges become narrower. Future work to achieve an improved theoretical understanding of the ELNES of these materials is required, particularly of the origin of features at the oxygen K-edge onset in the context of Hf-O coordination and the films' point defect chemistry. Such improved understanding would promote establishing relationships to the electrical and dielectric properties of gate dielectrics, which might be determined by the point defect chemistry.

Acknowledgements

This research was supported by the SRC/Sematech Front End Processing Center. S.S. acknowledges the use of the STEM facilities at the RRC at the University of Illinois at Chicago (NSF DMR-960172). We also acknowledge the use of the TEM facilities at the University of Houston MRSEC and NSF funding to upgrade the UH TEM (NSF-0076501).

References

Ahn, C.C. & Krivanek, O.L. (1983) *EELS Atlas*. Gatan Inc, Tempe/Warrendale.

Balmer, M.L., Lange, F.F. & Levi, C.G. (1994) Metastable Phase Selection and Partitioning for $Zr_{(1-x)}Al_xO_{(2-x/2)}$ Materials Synthesized with Liquid Precursors. *J. Am. Ceram. Soc.* **77**, 2069–2075.

de Boer, P.K. & de Groot, R.A. (1998) The conduction bands of MgO, MgS and HfO_2. *J. Phys. – Condensed Matter*, **10**, 10241–10248.

Busch, B.W., Pluchery, O., Chabal, Y.J., Muller, D.A., Opila, R.L., Kwo, J.R. & Garfunkel, E. (2002) Materials characterization of alternative gate dielectrics. *MRS Bull.* **27**, 206–211.

Camagni, P., Samoggia, G., Sangaletti, L., Parmigiani, F. & Zema, N. (1994) X-ray-photoelectron spectroscopy and optical reflectivity of yttrium-stabilized zirconia. *Phys. Rev. B*, **50**, 4292–4296.

Chen, J.G. (1997) NEXAFS investigations of transition metal oxides, nitrides, carbides, sulfides and other interstitial compounds. *Surf. Sci. Report*, **30**, 1–152.

Demkov, A.A. (2001) Investigating alternative gate dielectrics: a theoretical approach. *Phys. Stat. Sol. B*, **226**, 57–67.

van Dover, R.B., Lang, D.V., Green, M.L. & Manchanda, L. (2001) Crystallization kinetics in amorphous $(Zr_{0.62}Al_{0.38})\ O_{1.8}$ thin films. *J. Vac. Sci. Technol. A*, **19**, 2779–2784.

Egerton, R.F. (1996) *Electron Energy-Loss Spectroscopy in the Electron Microscope*. Plenum Press, New York.

French, R.H., Glass, S.J., Ohuchi, F.S., Xu, Y.N. & Ching, W.Y. (1994) Experimental and Theoretical Determination of the Electronic- Structure and Optical-Properties of 3 Phases of ZrO_2. *Phys. Rev. B*, **49**, 5133–5141.

Guo, X. (2001) Defect structure modification in zirconia by alumina. *Phys. Stat. Sol. (a)*, **183**, 261–271.

Hubbard, K.J. & Schlom, D.G. (1996) Thermodynamic stability of binary oxides in contact with silicon. *J. Mater. Res.* **11**, 2757–2776.

James, E.M., Browning, N.D., Nicholls, A.W., Kawasaki, M., Xin, Y. & Stemmer, S. (1998) Demonstration of atomic resolution Z-contrast imaging by a JEOL JEM-2010F scanning transmission electron microscope. *J. Electron Microsc.* **47**, 561–574.

Jomard, G., Petit, T., Pasturel, A., Magaud, L., Kesse, G. & Hafner, J. (1999) First-principles calculations to describe zirconia pseudopolymorphs. *Phys. Rev. B*, **59**, 4044–4052.

Kingon, A.I., Maria, J.P. & Streiffer, S.K. (2000) Alternative dielectrics to silicon dioxide for memory and logic devices. *Nature*, **406**, 1032–1038.

Kralik, B., Chang, E.K. & Louie, S.G. (1998) Structural properties and quasiparticle band structure of zirconia. *Phys. Rev. B*, **57**, 7027–7036.

Kwo, J., Hong, M., Kortan, A.R., Queeney, K.L., Chabal, Y.J., Opila, R.L., Muller, D.A., Chu, S.N.G., Sapjeta, B.J., Lay, T.S., Mannaerts, J.P., Boone, T., Krautter, H.W., Krajewski, J.J., Sergnt, A.M. & Rosamilia, J.M. (2001) Properties of high kappa gate dielectrics Gd_2O_3 and Y_2O_3 for Si. *J. Appl. Phys.* **89**, 3920–3927.

Lakiza, S.M. & Lopato, L.M. (1997) Stable and metastable phase relations in the system alumina-zirconia-yttria. *J. Am. Ceram. Soc.* **80**, 893–902.

Levi, C.G. (1998) Metastability and microstructure evolution in the synthesis of inorganics from precursors. *Acta Mater.* **46**, 787–800.

Lim, S.G., Kriventsov, S., Jackson, T.N., Haeni, J.H., Schlom, D.G., Balbashov, A.M., Uecker, R., Reiche, P., Freeouf, J.L. & Lucovsky, G. (2002) Dielectric functions and optical bandgaps of high-K dielectrics for metal-oxide-semiconductor field-effect transistors by far ultraviolet spectroscopic ellipsometry. *J. Appl. Phys.* **91**, 4500–4505.

Lucovsky, G. (2002) Correlations between electronic structure of transition metal atoms and performance of high-k gate dielectrics in advanced Si devices. *J. Non-Cryst. Solids*, **303**, 40–49.

Ma, T.P. (1998) Making silicon nitride film a viable gate dielectric. *IEEE Trans. Electron Dev.* **45**, 680–690.

McComb, D.W. (1996) Bonding and electronic structure in zirconia pseudopolymorphs investigated by electron energy-loss spectroscopy. *Phys. Rev. B*, **54**, 7094–7102.

McComb, D.W., Brydson, R., Hansen, P.L. & Payne, R.S. (1992) Qualitative interpretation of electron energy-loss near-edge structure in natural zircon. *J. Phys. Condens. Matter*, **4**, 8363–8374.

Medvedeva, N.I., Zhukov, V.P., Khodos, M.Y. & Gubanov, V.A. (1990) The electronic structure and cohesive energy of HfO_2, ZrO_2, TiO_2, and SnO_2 crystals. *Phys. Stat. Sol. (B)*, **160**, 517–527.

Neumayer, D.A. & Cartier, E. (2001) Materials characterization of ZrO_2-SiO_2 and HfO_2-SiO_2 binary oxides deposited by chemical solution deposition. *J. Appl. Phys.* **90**, 1801–1808.

Ostanin, S., Craven, A.J., McComb, D.W., Vlachos, D., Alavi, A., Finnis, M.W. & Paxton, A.T. (2000) Effect of relaxation on the oxygen K-edge electron energy-loss near-edge structure in yttria-stabilized zirconia. *Phys. Rev. B*, **62**, 14728–14735.

Ostanin, S., Craven, A.J., McComb, D.W., Vlachos, D., Alavi, A., Paxton, A.T. & Finnis, M.W. (2002) Electron energy-loss near-edge shape as a probe to investigate the stabilization of yttria-stabilized zirconia. *Phys. Rev. B*, **65**, 224109.

Otten, M.T. & Coene, W.M.J. (1993) High-resolution imaging on a field-emission TEM. *Ultramicroscopy*, **48**, 77–91.

Peacock, P.W. & Robertson, J. (2002) Band offsets and Schottky barrier heights of high dielectric constant oxides. *J. Appl. Phys.* **92**, 4712.

Ramanathan, S., Muller, D.A., Wilk, G.D., Park, C.M. & McIntyre, P.C. (2001) Effect of oxygen stoichiometry on the electrical properties of zirconia gate dielectrics. *Appl. Phys. Lett.* **79**, 3311–3313.

Rowley, P.N. & Graham, M.J. (1993) Characterization of high-temperature oxides using electron-energy loss spectroscopy. *Materials Performance*, **32**, 48–52.

Soriano, L., Abbate, M., Faber, J., Morant, C. & Sanz, J.M. (1995) The electronic-structure of ZrO_2 – band-structure calculations compared to electron and X-ray-spectra. *Solid State Commun.* **93**, 659–665.

Soriano, L., Abbate, M., Fuggle, J.C., Jimenez, M.A., Sanz, J.M., Mythen, C. & Padmore, H.A. (1993) The O 1s, X-ray absorption spectra of transition-metal oxides: the TiO_2-ZrO_2-HfO_2 and V_2O_5-Nb_2O_5-Ta_2O_5 series. *Solid State Commun.* **87**, 699–703.

Stemmer, S., Chen, Z., Keding, R., Maria, J.-P., Wicaksana, D. & Kingon, A.I. (2002) Stability of ZrO_2 layers on Si (001) during high-temperature anneals under reduced oxygen partial pressures. *J. Appl. Phys.* **92**, 82–86.

Suenaga, K., Bouchet, D., Colliex, C., Thorel, A. & Brandon, D.G. (1998) Investigations of alumina/spinel and alumina/zirconia interfaces by spatially resolved electron energy loss spectroscopy. *J. Eur. Ceram. Soc.* **18**, 1453–1459.

Vlachos, D., Craven, A.J. & McComb, D.W. (2001) The influence of dopant concentration on the oxygen K-edge ELNES and XANES in yttria-stabilized zirconia. *J. Phys. – Condens. Matter*, **13**, 10799–10809.

Wallis, D.J., Gaskell, P.H. & Brydson, R. (1995) Oxygen K near-edge spectra of amorphous silicon suboxides. *J. Microsc.* **180**, 307–312.

Wilk, G.D., Wallace, R.M. & Anthony, J.M. (2001) High-kappa gate dielectrics: current status and materials properties considerations. *J. Appl. Phys.* **89**, 5243–5275.

Wu, Z. & Seifert, F. (1996) Theoretical analysis of Si and O XANES spectra of zircon vs. alpha-quartz. *Solid State Commun.* **99**, 773–778.

Zhu, W.J., Ma, T.P., Di Tamagawa, T.Y., Kim, J., Carruthers, R., Gibson, M. & Furukawa, T. (2001) HfO_2 and HfAlO for CMOS: thermal stability and current transport. *IEDM Technical Digest*. art. no. 20–04.